Antimicrobial Delivery Using Metallophore-responsive Dynamic Nanocarriers

N.G. Hasitha Raviranga,[1] and Olof Ramström*[1,2]

[1]Department of Chemistry, University of Massachusetts Lowell, One University Ave., Lowell, MA 01854, USA;
Email: olof_ramstrom@uml.edu; [2]Department of Chemistry and Biomedical Sciences, Linnaeus University,
SE-39182 Kalmar, Sweden

Abstract: The increasing prevalence of multidrug-resistant (MDR) pathogens has promoted the development of innovative approaches, such as drug repurposing, synergy, and efficient delivery, in complement to traditional antibiotics. In this study, we present an approach based on biocompatible nanocarriers containing antimicrobial cations and known antibiotics. The matrices were prepared by coordinating Ga^{III} or In^{III} to formulations of chitosan/tripolyphosphate or catechol-functionalized chitosan, with or without encapsulated antibiotics, yielding particles of 100–200 nm hydrodynamic diameters. MDR clinical isolates of *P. aeruginosa* were found to be effectively inhibited by the nanocarriers under nutrient-limiting conditions. Fractional inhibitory concentration (FIC) indices revealed that cation- and antibiotic-encapsulated nanomatrices were effective against both Gram-negative and Gram-positive pathogens. Metallophores, such as deferoxamine (DFO) were probed to facilitate the sequestration and transport of the antimicrobial cations Ga^{III} or In^{III}. Although the antimicrobial activities were less significant with DFO, the eradication of biofilm-associated bacteria showed promising trends against *P. aeruginosa* and *S. epidermidis*. Interestingly, indium-containing compounds showed enhanced activity on biofilm formation and eradication, neutralizing *P. aeruginosa* under Fe-limiting conditions. In particular, In^{III}-crosslinked catechol-modified chitosan matrices were able to inhibit pathogenic growth together with DFO. The nanocarriers showed low cytotoxicity towards A549 cells and improvable CC_{50}-values with NIH/3T3 cells.

Introduction

The high rate of antibiotic resistance development has rendered many antimicrobials ineffective. Not only traditional antibiotics, such as penicillins or aminoglycosides, but also more contemporary antimicrobials, such as daptomycin and linezolid, are affected.[1] Since the drug discovery process requires a significant number of resources to identify and produce a single antibiotic, there is a potential that resistant isolates will have already emerged in the clinic by the time the drug reaches the market. A recent survey has shown that many pharmaceutical companies have abandoned the development of novel antibiotics and are engaged in the development of therapeutics that are more profitable.[2,3] Nonetheless, it appears that the COVID-19 pandemic has garnered the attention of numerous researchers, as the casualties arising from secondary infections have significantly impacted the mortality rate.[4,5] In the event of a sudden demand, antibiotic resistance would limit the capabilities of currently available drugs. Hence, researchers have explored more creative drug development strategies, such as identification of synergetic drug combinations,[6,7] drug repurposing,[8] and development of efficient drug carriers.[9] Such strategies may efficiently counter many infections, at least until more potent antibiotics reach the market.

Recently, the drug repurposing strategy has been extensively explored as it is anticipated to expedite the drug approval process.[10] For example, auranofin, an FDA-approved drug prescribed for rheumatoid arthritis, has been used against Gram-positive bacteria.[11] In

addition, analogues of this drug have been found to substantially inhibit the growth of both Gram-positive and Gram-negative bacteria, including *Pseudomonas aeruginosa*.[12,13] Another drug that has been repurposed as an antimicrobial agent is gallium nitrate (Ganite), which was originally prescribed for cancer-related hypercalcemia.[14] Gallium can for this purpose be used directly as the nitrate,[15] or in coordination complexes, such as Ga^{III}-porphyrins,[16] maltolate,[17] and citrate.[18] One reason for the antimicrobial activity of Ga^{III} is its similarity to Fe^{III}, which is an essential nutrient for microorganisms. Although the Ga^{III} cation shares a similar ionic radius as Fe^{III}, it does not share the redox capabilities of the Fe^{III}/Fe^{II} system under physiological conditions. This makes Ga^{III} a toxic substitute for Fe^{III} when entering the metabolic pathways of the microorganisms.[19] Microorganisms use specific metallophore virulence factors to sequester essential cations from the extracellular environment and to transport them through bacterial membrane channels.[20] Ga^{III} can hijack these processes and be internalized using Fe^{III}-selective metallophores (siderophores).

The multidrug-resistant (MDR) variants of the opportunistic pathogen *P. aeruginosa* are of special importance as they are responsible for nosocomial infections and numerous respiratory diseases. Currently, the US Centers for Disease Control and Prevention (CDC) categorizes *P. aeruginosa* under the serious threat category,[21] and new drugs and approaches to combat this pathogen need to be developed. The metallophore pathways can in principle be targeted for this purpose, where the most notable siderophores of *P. aeruginosa* are pyochelin and pyoverdine.[22] In addition to these, certain xenosiderophores are also capable of mediating the Fe^{III} uptake. For example, deferoxamine (DFO) can be internalized in *P. aeruginosa* via the outer membrane protein FoxA.[18,23] In this context, deferoxamine mesylate (Desferal) is an FDA-approved drug prescribed to treat iron toxicity.[24]

In addition to Ga^{III}, the antimicrobial activity of its group XIII companion In^{III} has also been reported.[25–27] In^{III} compounds that have been evaluated for this purpose include inorganic salts and metal-organic complexes based on ligands, such as porphyrins, phthalocyanins, or enterochelin.[28–31] Although the mechanism by which In^{III} inhibit bacterial growth is not known, it could possibly be due to the fact that the In^{III} ionic radius closely resembles that of Fe^{II}, which is about 0.62 Å,[32] thereby disrupting the bacterial iron homeostasis.

In addition to drug repurposing, the use of drug carriers for delivery and controlled release of antibiotic agents is a useful strategy to mitigate antimicrobial resistance. Among established drug carriers, such as liposomes, micelles, viral vectors, or polymeric particles,[33,34] recent studies have indicated that biocompatible polymer, such as chitosan or alginate, are suitable. The polycationic chitosan, derived from the structural polymer chitin found in many crustacean species, shows intrinsic antimicrobial potential, can be easily functionalized, and, most importantly, displays sustained drug release capability. Its inherent biodegradability also plays an important role in its use as a drug carrier.[35–39]

Another important method to counter bacterial growth is to identify synergetic drug combinations. Several well-known combinations are trimethoprim/sulfamethoxazole,[40] used to treat infections caused by *Pneumocystis jirovecii* (PCP), and amoxicillin/clavulanic acid against multidrug-resistant pathogens producing β-lactamases.[6] Synergetic combinations of DFO, Ga^{III}, and gentamicin have also been reported to reduce the planktonic and biofilm-associated growth of *P. aeruginosa*.[23]

In this study, we have synthesized chitosan nanoparticles that can coordinate the antimicrobial cations Ga^{III} and In^{III}, thereby enabling a sustained release at different pH levels. The antimicrobial activities of these compounds under different conditions were evaluated for

optimal administration. Similarly, chitosan cation-based nanomatrices containing co-encapsulated antibiotics were evaluated for potential synergistic antimicrobial effects. The possibility of enhancing the antimicrobial efficacy of the nanocarriers by introducing metallophores to trigger the uptake, rendering them more effective against biofilm-associated bacteria, was assessed. In addition, complexation of In^{III} ions with DFO rendered a new metal-based antimicrobial compound that shows activity against both planktonic and biofilm-associated bacteria. Furthermore, modification of chitosan with catechol groups paved the way towards a more defined cation coordination without additional crosslinking. Finally, the cytotoxic evaluation of these compounds was assessed with NIH/3T3 cells and A549 cells to identify possible preclinical candidates.

Results and Discussion

The chitosan nanoparticles (ChNPs) and cation-coordinated ChNPs (MChNPs) were synthesized by crosslinking low molecular weight (LMW) chitosan, 82% deacetylated as determined by ^{1}H-NMR (Figure S6), in the presence of sodium tripolyphosphate as depicted in **Figure 1**.[41,42] This ionic gelation method produced ChNPs in minutes, and the particles could be recovered using centrifugal filtration without any significant aggregation.

Figure 1. Synthesis of cation-coordinated chitosan nanoparticles (MChNPs).

The particles were characterized by DLS, showing hydrodynamic diameters in the range of 100–200 nm (Table S1). Although a direct correlation between the chitosan feed concentration and the particle size could not be discerned, the results suggest higher polydispersities with higher concentration of LMW chitosan. SEM analyses corroborated the DLS results, and also revealed the formation of larger particles (**Figure 2**). This could probably be due to aggregation of particles during the sample preparation steps of the SEM imaging. Thus, it was observed that solutions of the chitosan particles, similar to those of the parent non-crosslinked polymer, yielded a thin film over the silicon wafers used to immobilize the samples for imaging, rendering it difficult to locate particles.
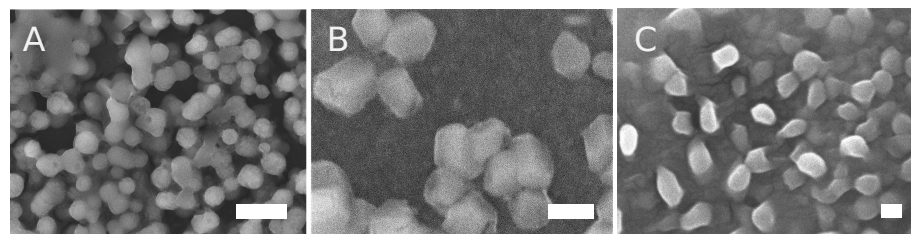

Figure 2. ChNPs (A; scale 1 μm) GaChNPs (B; scale 200 nm) InChNPs (C; scale 200 nm).

The cation coordination within the ChNP matrices was determined by ICP-MS, showing high degrees of metal incorporation into the particles: 84% for Ga^{III} and 72% for In^{III} (Table S2). This accounts for 32 μg Ga^{III}/mg ChNPs and 41 μg In^{III}/mg ChNPs, respectively (Table S3). The cation release kinetics was evaluated at two pH levels: 6.4 and 7.4, to evaluate the potential of sustained release of antimicrobial cations. For the GaChNPs, a significant cation

2 (14)

release could be observed within the first 6 hours at pH 7.4, while the release at pH 6.4 was less than half of this level during the same period (**Figure 3**A). However, after 48 hours, the cation release reached approximately 80% at both pH levels. Interestingly, a significant initial release was not observed at any pH level for the InChNPs, and the relative release the In^{III} was low compared to Ga^{III} (**Figure 3**B).
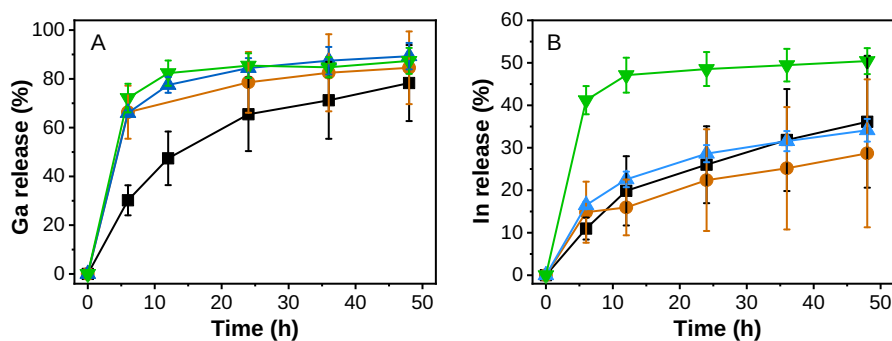

***Figure 3**. Cation release from GaChNPs (A) and InChNPs (B); pH 6.4, no DFO (black squares); pH 7.4, no DFO (orange circles); pH 6.4, DFO (blue triangles); pH 7.4, DFO (green triangles). Data represents mean ±SEM of two independent experiments (without DFO) and three independent experiments (with DFO).*

The metallophore DFO was next applied as a trigger to expedite the release and bacterial uptake of the cations. As depicted in **Figure 3**A, the Ga^{III} release was significantly increased with the introduction of DFO to the medium at pH 6.4, resulting in 66% release after 6 h and 90% after 48 h. Conversely, with InChNPs, the cation release was significantly accelerated at pH 7.4, resulting in >40% release within the first 6 h, and plateauing between 45-50% after 12 h (**Figure 3**B).

***Table 1:** Minimum inhibitory concentrations (MICs, µg/mL) of different antimicrobials in M9 minimal media or cation-adjusted Mueller-Hinton broth (CAMHB) at pH 6.5 or 7.3.[a]*

Antimicrobial	PAO1			27853		35984		AR 239			AR 241		
	M9	6.5	7.3	6.5	7.3	6.5	7.3	M9	6.5	7.3	M9	6.5	7.9
ChNPs	64	169	>169	>256	>256	64	>256	>256	>256	>256	>256	>256	>256
Ga(NO₃)₃	4	32	128	64	256	>256	>256	4	64/32	256	≤ 1	32	128
GaChNPs	32	158/79	>169	128	>256	32	>256	16	256	>256	8	256	>256
In(NO₃)₃	4	32[b]	32[b]	>256	>256	>256	>256	32	>256	>256	≤ 1	>256	>256
InChNPs	16	150/75	38/19[b]	256	>256	32	256	32	>256	>256	≤ 1	>256	>256
Gentamicin	0.5	2	2	2	2	>64	32	>64	>64	>64	>64	64	64

[a]PAO1: *P. aeruginosa* PAO1; 27853: *P. aeruginosa* ATCC 27853; 35984: *S. epidermidis* ATCC 35984; AR 239 and AR 241: MDR isolates. All results repeated at least twice in triplicates; highest MIC value or mode of trials tabulated; [b]MICs observed with trailing turbidities.

The antimicrobial activity of the particles was assessed in iron-rich CAMHB media at pH 6.5 and 7.3, as well as in M9 minimal media, with different strains of *P. aeruginosa* and *S. epidermidis*. As shown in **Table 1**, none of the pseudomonal strains except PAO1 showed any growth inhibition in the presence of the metal ion-free ChNPs under all tested conditions. In contrast, the inhibition of the growth of *P. aeruginosa* PAO1 was most prominent with the InChNPs in M9 media, and the growth of *P. aeruginosa* ATCC 27853 was inhibited with GaChNPs in pH 6.5 CAMHB. Two *P. aeruginosa* MDR isolates, AR 239 and AR 241, chosen from the AR isolate bank were also probed, being resistant towards most antibiotics in

comparison to other isolates in the panel. For example, the MDR isolates are resistant towards gentamicin, one of the most potent antibiotics administered in healthcare facilities against severe infections. The resistance profile and their resistance mechanisms are summarized in Table S4–S5. Interestingly, these MDR isolates showed significant sensitivity towards both MChNPs when grown in M9 media. This could be due to an increase in cation uptake or a decrease in the activity of efflux pumps, resulting in net buildup of the antimicrobial cations for a longer residence time in the pathogens. In comparison, the MChNPs were not significantly active against the Gram-positive pathogen *Staphylococcus epidermidis* ATCC 35984.

Table 2: *MICs (µg/mL) of different antimicrobials in Fe-poor CAMHB at pH 6.5 or 7.3.[a]*

Antimicrobial	PAO1[a]		27853[a]		35984[b]	
	6.5	7.3	6.5	7.3	6.5	7.3
ChNP	169/85	>169	256	>256	32	>256
Ga(NO$_3$)$_3$	16	64/32	16	128	>256	>256
GaChNPs	158/79	>149	64	256	32	>256
In(NO$_3$)$_3$	≤ 1	2	>256	>256	>256	>256
InChNPs	5/2.5	9/4.7	64/32	256	32	>256
Gentamicin	4	4	2	2	>64	32

[a]Cultures grown overnight in CAMHB supplemented with 64 µg/ml bpy before challenging with antimicrobials in same media; [b]cultures grown overnight in CAMHB supplemented with 8 µg/ml bpy before challenging with antimicrobials in same media; PAO1: *P. aeruginosa* PAO1; 27853: *P. aeruginosa* ATCC 27853; 35984: *S. epidermidis* ATCC 35984. All results repeated at least twice in triplicates; highest MIC value or mode of trials tabulated.

Since the antimicrobial activities of MChNPs were more pronounced in M9 media, cultured bacteria were also treated with the Fe[III]-quencher 2,2'-bipyridine (bpy), supplemented to CAMHB, to evaluate whether a similar effect can be achieved in nutrient-rich media. Each culture was treated with at least 4-times lower concentration of bpy than its MICs for each pathogen. Interestingly, a significant bacterial inhibition was achieved in *P. aeruginosa* cultures challenged with InChNP or In(NO$_3$)$_3$, while *S. epidermidis* remained resilient towards both cations (**Table 2**). Although *P. aeruginosa* ATCC 27853 was more resistant towards the MChNPs in the absence of bpy (**Table 1**), the bpy-supplemented media creates an environment where the pathogen is more susceptible towards these cations. In comparison, the inhibition of *S. epidermidis* was mainly due to the intrinsic antimicrobial activity of chitosan.

We next addressed the potential of encapsulating known antibiotics in the nanocarriers to achieve synergistic responses in conjunction with the activity of the metal ions. Antibiotics that can affect the ion/electrolyte balance across fungal/bacterial membranes were in this case chosen: amphotericin B, typically prescribed for fungal infections, as well as valinomycin and gramicidin, both capable of transporting cations across cell membranes leading to pathogenic cell death. The antibiotics were encapsulated in the Ga[III]- or In[III]-ChNPs and MICs and fractional inhibitory concentration indices (FICIs) were determined for each combination (**Table 3**).

For *P. aeruginosa* PAO1, the effects of the antibiotics were most significant when encapsulated in the InChNPs. The combination between In[III] and amphotericin B successfully inhibited the growth of *P. aeruginosa* PAO1 with an FICI of 0.12. An FICI of ≤ 0.5 is considered synergistic, and this indicates significant synergy between the antibiotic and the metal ion. Clear effects with Ga[III] could in this case not be discerned. In contrast, neither combination affected *S. epidermidis* ATCC 35984 to any significant degree within the tested

range. Similar results were obtained for valinomycin and gramicidin, and the combinations with In^{III} yielded the strongest synergy effects with *P. aeruginosa* PAO1. However, in these cases the combinations with Ga^{III} also resulted in low FICIs (0.33), although the overall antimicrobial activity was lower than for In^{III}. Both metal ions showed strong synergistic effects together with gramicidin against *S. epidermidis* ATCC 35984, whereas no results for valinomycin could be determined. Overall, these results indicate that administration of encapsulated antibiotics in Ga^{III}- or In^{III}-ChNPs can lead to enhanced antimicrobial activity against *P. aeruginosa* PAO1 and *S. epidermidis* ATCC 35984.

Table 3: *Synergistic antimicrobial approach using antibiotics and cations encapsulated in ChNPs against P. aeruginosa PAO1 and S. epidermidis ATCC 35984.*

	P. aeruginosa PAO1				*S. epidermidis* ATCC 35984			
	MIC (μg/mL)	antibiotic[a] (μg/mL)	cation[a] (μg/mL)	FICI (synergy)	MIC (μg/mL)	antibiotic[a] (μg/mL)	cation[a] (μg/mL)	FICI (synergy)
Amphotericin B	>128	-	-	-	>128	-	-	-
ABGaChNP[b]	N.R.	N.R.	N.R.	N.R.	N.R.	N.R.	N.R.	N.R.
ABInChNP	16	0.014	0.66	0.12	>128	>0.112	>5.30	N.D.
Valinomycin	>32	-	-	-	>32	-	-	-
VLGaChNP	64	0.056	2.07	0.33	>128	>0.112	>4.14	N.D.
VLInChNP	16/8	0.014/0.007	0.66/0.33	0.13	>128	>0.112	>5.30	N.D.
Gramicidin	>32	-	-	-	8/4	-	-	-
GRGaChNP	64	0.056	2.07	0.33	8	0.007	2.07	0.11
GRInChNP	8	0.007	0.33	0.06	16	0.014	0.33	0.10

[a]Approximate concentrations at MIC based on concentration as estimated in Table S7; [b]no evidence of particle formation; N.R.: no clear results recorded; N.D.: not determined.

A main purpose of MChNPs is to serve as reservoirs of antibiotic cations, allowing either naturally secreted bacterial siderophores or exogenously added metallophores to mediate their transport across the bacterial membranes as depicted in **Figure 4**. The triggered release response of MChNPs demonstrated the ability of DFO to strip Ga^{III} and In^{III} from MChNPs (**Figure 3**). To gain more information regarding the metallophore effects, checkerboard analyses of the MChNPs or the metal ion nitrates, together with DFO, were performed in M9 or CAMHB media. The analyses revealed an interesting interplay between the species *in vitro*. Thus, Ga^{III} displayed a tendency to act in an antagonistic relationship with DFO (Figure S10–S11), regardless of being administered in MChNP-form or as nitrate. Although Ga^{III} shows close resemblance to Fe^{III} in terms of size and coordination pattern, this observation suggests that Ga^{III} is bound by DFO, but that the complex may not be efficiently internalized by planktonic *P. aeruginosa*. The same effect could also be recorded with the drug deferiprone (DFP, Figure S12–S13), an Fe^{III} chelator prescribed to remove excess iron from the body in patients with anemia, thalassemia and sickle cell disease. However, the checkerboard analysis of the In^{III}-containing species showed additive effects (InChNPs) or synergistic effects (In(NO$_3$)$_3$) in contrast to the Ga^{III} counterpart.
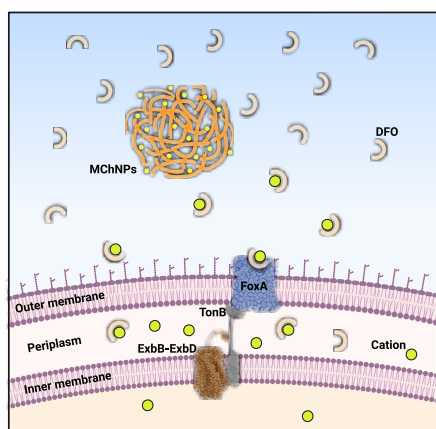
Figure 4. *MChNPs serving as a cation reservoir for metallophore complexation and uptake by virulent pathogens. Created with BioRender.com*

As described in a previous study, where biofilm eradication was achieved with Ga^III, DFO, and additional antibiotics,[23] the environment of the pathogen is crucial for the uptake of the metallophore complex. To test this, we also evaluated the effects of the MChNPs toward biofilm eradication against *P. aeruginosa* in the presence and absence of DFO (**Figure 5**). Interestingly, the studies revealed that co-administration with DFO was effective and both the GaChNPs and the InChNPs showed improved inhibitory trends relative to being administered without DFO. In addition, although the metal ion-containing nanocarriers did not demonstrate any substantial inhibitory effects against *S. epidermidis* planktonic bacteria (**Table 1**), the MChNPs showed significant antibiofilm effects as depicted in **Figure 6**.
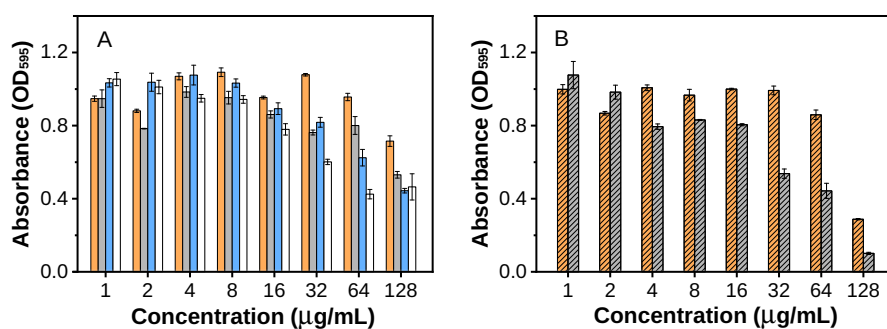

Figure 5. *P. aeruginosa PAO1 biofilm eradication; A) nanocarriers or nitrates only; B) MChNPs in the presence of DFO (250 µg/mL); GaChNPs (orange), InChNPs (grey), Ga(NO$_3$)$_3$ (blue), In(NO$_3$)$_3$ (white), GaChNPs with DFO (patterned orange), InChNPs with DFO (patterned grey).*
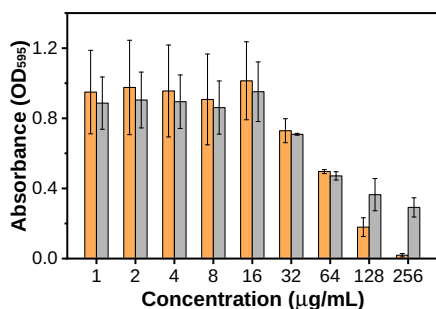
Figure 6. *Biofilm eradication of S. epidermidis ATCC 35984; GaChNPs (orange), InChNPs (grey).*

To further evaluate the additive or synergistic effects between In^{III} and DFO observed in the checkerboard experiments (Figure S10–S11) and the results from the biofilm eradication experiments, the In-DFO complex was synthesized as shown in **Figure 7**. The complex was tested against *P. aeruginosa* PAO1, and compared with the effects from InChNPs or In(NO$_3$)$_3$ in the presence of DFO (**Table 4**). Although the inhibitory effects of the complex were not significantly improved compared to administering In^{III} through InChNPs and DFO, a clearer MIC point was observed with In-DFO than the trailing MIC observed for other In^{III}-based compounds. This suggests that a trailing MIC represents the occurrence of a more bacteriostatic effect after the MIC point, whereas the In-DFO complex results in a more direct bactericidal effect. On the other hand, the observed antibiofilm effects against *P. aeruginosa* biofilms established over 24 h were somewhat similar to InChNPs with DFO (**Figure 8**).
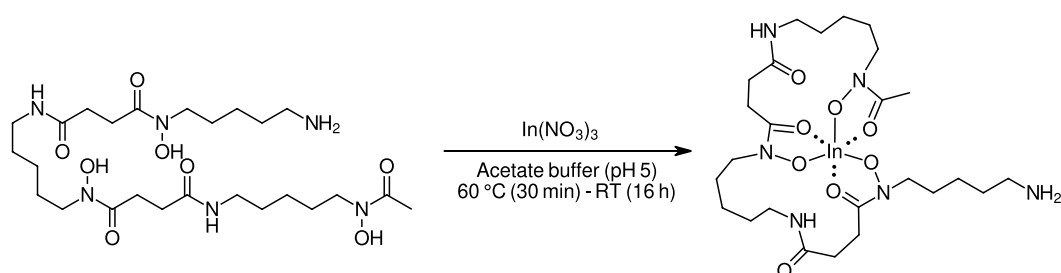

Figure 7. *Synthesis of In-DFO*

Table 4: *MICs (µg/mL) of In-DFO against P. aeruginosa PAO1[a].*

	CAMHB pH 6.5	**CAMHB pH 7.3**	**M9**
In(NO$_3$)$_3$	32[b]	32[b]	4
InChNPs	16	150/75	38/19[b]
In-DFO	128/64	64	128/64

[a]Cultures grown overnight in CAMHB supplemented with 64 µg/ml bpy before challenging with antimicrobials in same media; [b]Trailing MICs.
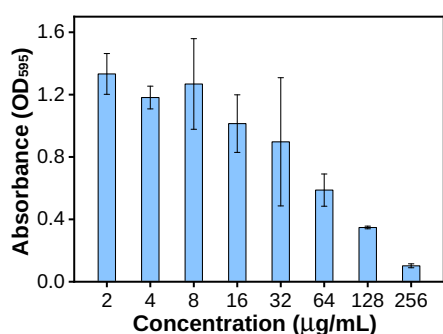
Figure 8: P. aeruginosa PAO1 biofilm eradication using In-DFO

Since the coordination of cations within the ChNPs is not structurally well-defined, catechol-functionalized chitosan (CCh) was synthesized from LMW chitosan (82% deacetylated) through reductive amination with 3,4-dihydroxybenzaldehyde (**Figure 9**).[43] Analysis by ^{1}H-NMR yielded a catechol substitution rate of 91% (**Figure 10**B), resulting in an approximate 11:1:3 ratio of catechol-modified amine groups, free amine groups, and acetylated amine groups. Based on this, Ga[III]- or In[III]-crosslinked CCh, having 2 or 3 catechol groups per cation, could be prepared as illustrated in **Figure 10**A.
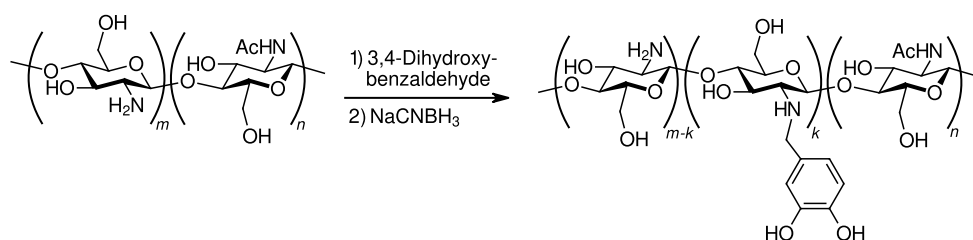

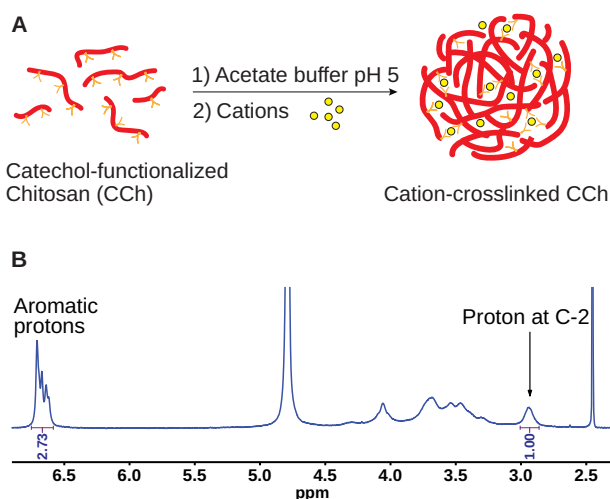*Figure 9. Synthesis of catechol-functionalized chitosan.*

Figure 10. Schematic representation of cation-crosslinked CCh (A); ^{1}H-NMR spectrum of catechol-functionalized chitosan (CCh, B).

The crosslinking process yielded hydrogels and particles that were observable as aggregates. However, approaches to achieve particles of similar size as the previously prepared ChNPs was not successful. In addition, since catechols are sensitive to air exposure for longer periods, these matrices were primarily evaluated for growth inhibition effects in 96-well microtiter

8 (14)

plates. Briefly, catechol-functionalized chitosan was mixed with the cations in each well at a defined ratio, and the mixture was treated with NH_4OH to initiate gelation.[44] Drying, rinsing, and rehydration yielded the final surface-bound hydrogels, to which a *P. aeruginosa* PAO1 culture of 5×10^5 CFU/mL with either DFO or DFP was introduced and allowed to grow for 27 h (Figure S14). The results were conspicuous, and InCCh was able to completely inhibit the bacterial growth in the presence of DFO. This suggests that cation-crosslinked CCh can act as a surface-adhesive and a cation source that is able to release antimicrobial cations upon metallophore introduction.

The capability of the MCCh gels to inhibit biofilm formation of *P. aeruginosa* or *S. epidermidis* was assessed using a similar approach (Figure S15). Of the bacterial strains, the biofilm formation by *S. epidermidis* was more effectively inhibited than that of *P. aeruginosa*. This could be due to the fact that *P. aeruginosa* forms biofilms at the air-liquid interface while biofilms of *S. epidermidis* are mostly confined at the bottom of the wells. The inhibitory effect of the MCCh gels also decreased when increasing the ratio of CCh, both at pH 6.5 or pH 7.3. This effect was especially noticeable with *P. aeruginosa* PAO1, and *P. aeruginosa* is known to form heavy biofilms in Ga^{III}-containing media.[45] Altogether, the results suggest that without the metallophore the inhibitory effects of MCCh could not be achieved.

To evaluate the cytotoxicity effects of the established matrices, tests on NIH/3T3 and A549 cells were performed. In both cases, CC_{50}-values for the ChNPs or MChNPs could not be determined, in part due to limitations in solubility and unclear transitions at high concentrations. Nevertheless, within the concentration window, the cells remained metabolically >50% active, relative to the growth control, indicating CC_{50}-values >256 μg/mL. On the other hand, the cytotoxicity of the CCh preparation was relatively high, with CC_{50}-values of 36 μg/mL on 3T3-cells and 80 μg/mL for A549 cells (Figure S16–S17), albeit likely due to a high acetic acid content (15%) in the samples. An estimated CC_{50}-value of >70 μg/mL were recorded for $Ga(NO_3)_3$ on 3T3 cells, whereas no reliable data for $In(NO_3)_3$ could be obtained (Figure S16). Interestingly, the viability of the A549 cells were not significantly affected by any of the compounds, except CCh, as depicted in **Figure 11** and summarized in **Table 5**.
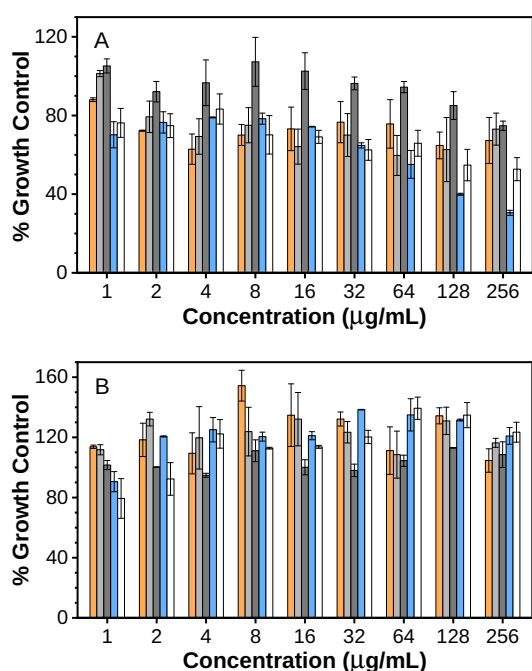
Figure 11. *Cytotoxicity on NIH/3T3 fibroblast cells (A), and human alveolar A549 cells (B). GaChNPs (orange), InChNPs (grey), ChNPs (dark grey), $Ga(NO_3)_3$ (blue), $In(NO_3)_3$ (white).*

Table 5: *Comparison of MIC-values against P. aeruginosa PAO1 and corresponding CC_{50} values for NIH/3T3 and A549 cells.*

	MICs against PAO1		CC_{50}	
	6.5	**7.3**	**NIH/3T3**	**A549**
ChNP	169	>169	N.D.	>256
GaChNP	158/79	>169	>256	>256
InChNP	150/75	38/19[a]	>256	>256
$Ga(NO_3)_3$	32	128	>70	>256
$In(NO_3)_3$	32[a]	32[a]	N.D.	>256
CCh	-	-	36	80

[a]Trailing MICs; N.D.: not determined.

Conclusions

We have shown that chitosan-based nanoparticles in the 100-200 nm diameter range can be synthesized using a straightforward method. The particles could accommodate satisfactory levels of cations, allowing them to act as vessels for the delivery of antimicrobials. The particles showed sustained cation-release, that could be triggered by the introduction of metallophores such as DFO. The activity of the MChNPs under different culturing conditions and against different bacterial strains suggests optimal administration methods for particular bacterial strains. Importantly, high antimicrobial activity against MDR *P. aeruginosa* clinical isolates could be demonstrated in M9 minimal media, suggesting that the pathogenicity of the isolates can be mitigated using this nanocarrier approach. Moreover, under nutrient-rich, iron-limited conditions, the InChNPs caused significant bacterial inhibition. Decisive synergistic

effects could be recorded by encapsulating antibiotics within the nanocarriers, as exemplified using membrane-disrupting antibiotic species in conjunction with the cation release. Furthermore, bacterial biofilms could be eradicated using the nanocarriers in the presence of metallophores, such as DFO, an effect especially prominent with the InChNPs. A discrete In-DFO complex was also synthesized and evaluated, suggesting a stronger bactericidal effect in contrast to the potentially bacteriostatic inhibition by the InChNPs and $In(NO_3)_3$ against *P. aeruginosa*. Catechol-functionalized chitosan was able to crosslink through a cation-assisted mechanism and enabled a bactericidal effect against *P. aeruginosa* together with DFO. The cytotoxicities of the different compounds were dependent on the cell lines, and indicate, together with the FICIs and the antibiofilm data, proper dosing regimes.

Author Information

Corresponding author

Olof Ramström; E-mail: olof_ramstrom@uml.edu

Acknowledgements

Keywords

P. aeruginosa, antimicrobial, nanocarriers, gallium, indium, chitosan

REFERENCES

(1) Lowy, F. D. Antimicrobial Resistance: The Example of *Staphylococcus aureus*. *J. Clin. Invest.* **2003**, *111*, 1265–1273. https://doi.org/10.1172/JCI18535.

(2) Plackett, B. Why Big Pharma Has Abandoned Antibiotics. *Nat. Outlook* **2020**, *586*, 50–52.

(3) Ventola, C. L. The Antibiotic Resistance Crisis: Part 1: Causes and Threats. *P T* **2015**, *40*, 277–283.

(4) Lastinger, L. M.; Alvarez, C. R.; Kofman, A.; Konnor, R. Y.; Kuhar, D. T.; Nkwata, A.; Patel, P. R.; Pattabiraman, V.; Xu, S. Y.; Dudeck, M. A. Continued Increases in the Incidence of Healthcare-Associated Infection (HAI) During the Second Year of the Coronavirus Disease 2019 (COVID-19) Pandemic. *Infect. Control Hosp. Epidemiol.* **2022**, *44*, 997–1001. https://doi.org/10.1017/ice.2022.116.

(5) NCEZID/CDC. *COVID-19: U.S. Impact on Antimicrobial Resistance, Special Report 2022*; National Center for Emerging and Zoonotic Infectious Diseases, 2022. https://doi.org/10.15620/cdc:117915.

(6) Drago, L.; Nicola, L.; Rodighiero, V.; Larosa, M.; Mattina, R.; Vecchi, E. Comparative Evaluation of Synergy of Combinations of β-Lactams with Fluoroquinolones or a Macrolide in *Streptococcus pneumoniae*. *J. Antimicrob. Chemother.* **2011**, *66*, 845–849. https://doi.org/10.1093/jac/dkr016.

(7) Daley, D.; Mulgrave, L.; Munro, R.; Neville, S.; Smith, H.; Dimech, W. An Evaluation of the in Vitro Activity of Piperacillin/Tazobactam. *Pathology* **1996**, *28*, 167–172. https://doi.org/10.1080/00313029600169813.

(8) Boyd, N. K.; Teng, C.; Frei, C. R. Brief Overview of Approaches and Challenges in New Antibiotic Development: A Focus on Drug Repurposing. *Front. Cell. Infect. Microbiol.* **2021**, *11*. https://doi.org/10.3389/fcimb.2021.684515.

(9) Finbloom, J. A.; Sousa, F.; Stevens, M. M.; Desai, T. A. Engineering the Drug Carrier Biointerface to Overcome Biological Barriers to Drug Delivery. *Adv. Drug Deliv. Rev.* **2020**, *167*, 89–108. https://doi.org/10.1016/j.addr.2020.06.007.

(10) Farha, M. A.; Brown, E. D. Drug Repurposing for Antimicrobial Discovery. *Nat. Microbiol.* **2019**, *4*,

(11) Harbut, M. B.; Vilchèze, C.; Luo, X.; Hensler, M. E.; Guo, H.; Yang, B.; Chatterjee, A. K.; Nizet, V.; Jacobs, W. R.; Schultz, P. G.; Wang, F. Auranofin Exerts Broad-Spectrum Bactericidal Activities by Targeting Thiol-Redox Homeostasis. *Proc. Natl. Acad. Sci. U. S. A.* **2015**, *112*, 4453–4458. https://doi.org/10.1073/pnas.1504022112.

(12) Ndugire, W.; Truong, D.; Raviranga, N. G. H.; Lao, J.; Ramström, O.; Yan, M. Turning on the Antimicrobial Activity of Gold Nanoclusters Against Multidrug-Resistant Bacteria. *Angew. Chem. Int. Ed.* **2023**, *62*, 202214086. https://doi.org/10.1002/anie.202214086.

(13) Ndugire, W.; Raviranga, N. G. H.; Lao, J.; Ramström, O.; Yan, M. Gold Nanoclusters as Nanoantibiotic Auranofin Analogues. *Adv. Healthc. Mater.* **2022**, *11*, 2101032. https://doi.org/10.1002/adhm.202101032.

(14) Bonchi, C.; Imperi, F.; Minandri, F.; Visca, P.; Frangipani, E. Repurposing of Gallium-Based Drugs for Antibacterial Therapy. *BioFactors* **2014**, *40*, 303–312. https://doi.org/10.1002/biof.1159.

(15) Kaneko, Y.; Thoendel, M.; Olakanmi, O.; Britigan, B. E.; Singh, P. K. The Transition Metal Gallium Disrupts *Pseudomonas aeruginosa* Iron Metabolism and Has Antimicrobial and Antibiofilm Activity. *J. Clin. Invest.* **2007**, *117*, 877–888. https://doi.org/10.1172/JCI30783.

(16) Hijazi, S.; Visca, P.; Frangipani, E. Gallium-Protoporphyrin IX Inhibits *Pseudomonas aeruginosa* Growth by Targeting Cytochromes. *Front. Cell. Infect. Microbiol.* **2017**, *7*, 1–15. https://doi.org/10.3389/fcimb.2017.00012.

(17) Baldoni, D.; Steinhuber, A.; Zimmerli, W.; Trampuz, A. In Vitro Activity of Gallium Maltolate Against Staphylococci in Logarithmic, Stationary, and Biofilm Growth Phases: Comparison of Conventional and Calorimetric Susceptibility Testing Methods. *Antimicrob. Agents Chemother.* **2010**, *54*, 157–163. https://doi.org/10.1128/AAC.00700-09.

(18) Rzhepishevska, O.; Ekstrand-Hammarström, B.; Popp, M.; Björn, E.; Bucht, A.; Sjöstedt, A.; Antti, H.; Ramstedt, M. The Antibacterial Activity of Ga³⁺ Is Influenced by Ligand Complexation as Well as the Bacterial Carbon Source. *Antimicrob. Agents Chemother.* **2011**, *55*, 5568–5580. https://doi.org/10.1128/AAC.00386-11.

(19) Weaver, K. D.; Heymann, J. J.; Mehta, A.; Roulhac, P. L.; Anderson, D. S.; Nowalk, A. J.; Adhikari, P.; Mietzner, T. A.; Fitzgerald, M. C.; Crumbliss, A. L. Ga³⁺ as a Mechanistic Probe in Fe³⁺ Transport: Characterization of Ga³⁺ Interaction with FbpA. *J. Biol. Inorg. Chem.* **2008**, *13*, 887–898. https://doi.org/10.1007/s00775-008-0376-5.

(20) Hider, R. C.; Kong, X. Chemistry and Biology of Siderophores. *Nat. Prod. Rep.* **2010**, *27*, 637–657. https://doi.org/10.1039/b906679a.

(21) CDC. *Antibiotic resistance threats in the United States 2019*; research report; Centers for Disease Control and Prevention, US Department of Health and Human Services, 2019; pp 1–148.

(22) Lamont, I. L.; Beare, P. A.; Ochsner, U.; Vasil, A. I.; Vasil, M. L. Siderophore-Mediated Signaling Regulates Virulence Factor Production in *Pseudomonas aeruginosa*. *Proc. Natl. Acad. Sci. U. S. A.* **2002**, *99*, 7072–7077. https://doi.org/10.1073/pnas.092016999.

(23) Banin, E.; Lozinski, A.; Brady, K. M.; Berenshtein, E.; Butterfield, P. W.; Moshe, M.; Chevion, M.; Greenberg, E. P.; Banin, E. The Potential of Desferrioxamine-Gallium as an Anti-Pseudomonas Therapeutic Agent. *Proc. Natl. Acad. Sci. U. S. A.* **2008**, *105*, 16761–16766. https://doi.org/10.1073/pnas.0808608105.

(24) Brittenham, G. M.; Griffith, P. M.; Nienhuis, A. W.; McLaren, C. E.; Young, N. S.; Tucker, E. E.; Allen, C. J.; Farrell, D. E.; Harris, J. W. Efficacy of Deferoxamine in Preventing Complications of Iron Overload in Patients with Thalassemia Major. n. *N. Engl. J. Med.* **1994**, *331*, 567–573. https://doi.org/10.1056/nejm199409013310902.

(25) Soy, R. C.; Babu, B.; Oluwole, D. O.; Nwaji, N.; Oyim, J.; Amuhaya, E.; Prinsloo, E.; Mack, J.; Nyokong, T. Photophysicochemical Properties and Photodynamic Therapy Activity of Chloroindium(III) Tetraarylporphyrins and Their Gold Nanoparticle Conjugates. *J. Porphyrins Phthalocyanines* **2019**, *23*, 34–45. https://doi.org/10.1142/S1088424618501146.

(26) Tajbakhsh, S.; Mohammadi, K.; Deilami, I.; Zandi, K.; Fouladvand, M.; Ramedani, E.; Asayesh, G. Antibacterial Activity of Indium Curcumin and Indium Diacetylcurcumin. *African J. Biotechnol.* **2008**, *7*, 3832–3835. https://doi.org/10.5897/AJB08.790.

(27) David, S.; Barros, V.; Cruz, C.; Delgado, R. In Vitro Effect of Free and Complexed Indium(III) Against *Mycobacterium tuberculosis*. *FEMS Microbiol. Lett.* **2005**, *251*, 119–124. https://doi.org/10.1016/j.femsle.2005.07.044.

(28) Sen, P.; Mack, J.; Nyokong, T. Indium Phthalocyanines: Comparative Photophysicochemical Properties and

(29) Bozja, J.; Yi, K.; Shafer, W. M.; Stojiljkovic, I. Porphyrin-Based Compounds Exert Antibacterial Action Against the Sexually Transmitted Pathogens *Neisseria gonorrhoeae* and *Haemophilus ducreyi*. *Int. J. Antimicrob. Agents* **2004**, *24*, 578–584. https://doi.org/10.1016/j.ijantimicag.2004.06.008.

(30) Rogers, H. J.; Synge, C.; Woods, V. E. Antibacterial Effect of Scandium and Indium Complexes of Enterochelin on *Klebsiella pneumoniae*. *Antimicrob. Agents Chemother.* **1980**, *18*, 63–68. https://doi.org/10.1128/aac.18.1.63.

(31) Jahnel, F. Chemotherapeutic Properties of Indium in Experimental Syphilis and Trypanosomiasis. *Z. Immunitätsforsch.* **1940**, *98*, 112–123.

(32) Shannon, R. D. Revised Effective Ionic Radii and Systematic Studies of Interatomic Distances in Halides and Chalcogenides. *Acta Crystallogr. Sect. A* **1976**, *32*, 751–767. https://doi.org/10.1107/S0567739476001551.

(33) Long, Y.; Li, Z.; Bi, Q.; Deng, C.; Chen, Z.; Bhattachayya, S.; Li, C. Novel Polymeric Nanoparticles Targeting the Lipopolysaccharides of *Pseudomonas aeruginosa*. *Int. J. Pharm.* **2016**, *502*, 232–241. https://doi.org/10.1016/j.ijpharm.2016.02.021.

(34) Wilczewska, A. Z.; Niemirowicz, K.; Markiewicz, K. H.; Car, H. Nanoparticles as Drug Delivery Systems. *Pharmacol. Rep.* **2012**, *64*, 1020–1037. https://doi.org/10.1016/s1734-1140(12)70901-5.

(35) Asadi, S.; Mortezagholi, B.; Hadizadeh, A.; Borisov, V.; Ansari, M. J.; Majdi, H. S.; Nishonova, A.; Adelnia, H.; Far, B. F.; Chaiyasut, C. Ciprofloxacin-Loaded Titanium Nanotubes Coated with Chitosan: A Promising Formulation with Sustained Release and Enhanced Antibacterial Properties. *Pharmaceutics* **2022**, *14*, 1359. https://doi.org/10.3390/pharmaceutics14071359.

(36) Gheorghita, R.; Anchidin-Norocel, L.; Filip, R.; Dimian, M.; Covasa, M. Applications of Biopolymers for Drugs and Probiotics Delivery. *Polymers* **2021**, *13*, 2729. https://doi.org/10.3390/polym13162729.

(37) Kamaruzzaman, N. F.; Tan, L. P.; Hamdan, R. H.; Choong, S. S.; Wong, W. K.; Gibson, A. J.; Chivu, A.; Fatima Pina, M. de. Antimicrobial Polymers: The Potential Replacement of Existing Antibiotics? *Int. J. Mol. Sci.* **2019**, *20*, 2747. https://doi.org/10.3390/ijms20112747.

(38) Uskoković, V.; Desai, T. A. In Vitro Analysis of Nanoparticulate Hydroxyapatite/Chitosan Composites as Potential Drug Delivery Platforms for the Sustained Release of Antibiotics in the Treatment of Osteomyelitis. *J. Pharm. Sci.* **2014**, *103*, 567–579. https://doi.org/10.1002/jps.23824.

(39) Oungbho, K.; Müller, B. W. Chitosan Sponges as Sustained Release Drug Carriers. *Int. J. Pharm.* **1997**, *156*, 229–237. https://doi.org/10.1016/s0378-5173(97)00201-9.

(40) Bush, K. *Synergistic Antibiotic Combinations BT - Antibacterials*; Fisher, J. F., Mobashery, S., Miller, M. J., Eds.; Springer International Publishing: Cham, 2018; Vol. I, pp 69–88. https://doi.org/10.1007/7355_2017_23.

(41) Fan, W.; Yan, W.; Xu, Z.; Ni, H. Formation Mechanism of Monodisperse, Low Molecular Weight Chitosan Nanoparticles by Ionic Gelation Technique. *Colloids Surf., B* **2012**, *90*, 21–27. https://doi.org/10.1016/j.colsurfb.2011.09.042.

(42) Ali, S. W.; Rajendran, S.; Joshi, M. Synthesis and Characterization of Chitosan and Silver Loaded Chitosan Nanoparticles for Bioactive Polyester. *Carbohydr. Polym.* **2011**, *83*, 438–446. https://doi.org/10.1016/j.carbpol.2010.08.004.

(43) Guo, Z.; Ni, K.; Wei, D.; Ren, Y. Fe^{III}-Induced Oxidation and Coordination Cross-Linking in Catecholchitosan Hydrogels Under Acidic pH Conditions. *RSC Adv.* **2015**, *5*, 37377–37384. https://doi.org/10.1039/c5ra03851k.

(44) Ryu, J. H.; Hong, S.; Lee, H. Bio-Inspired Adhesive Catechol-Conjugated Chitosan for Biomedical Applications: A Mini Review. *Acta Biomater.* **2015**, *27*, 101–115. https://doi.org/10.1016/j.actbio.2015.08.043.

(45) García-Contreras, R.; Pérez-Eretza, B.; Lira-Silva, E.; Jasso-Chávez, R.; Coria-Jiménez, R.; Rangel-Vega, A.; Maeda, T.; Wood, T. K. Gallium Induces the Production of Virulence Factors in *Pseudomonas aeruginosa*. *Pathog. Dis.* **2014**, *70*, 95–98. https://doi.org/10.1111/2049-632x.12105.